scientific reports

Check for updates

OPEN

Deep learning assisted prediction of microstructure and wear behaviour in plasma nitrided 316 L stainless steel

K. Thavasilingam[1], S. Velmurugan[2], M. Prashanth[3], R. Selva Bharathi[4], S. Thirumalai Kumaran[5], R. Sundarakannan[6]✉ & M. Uthayakumar[7]✉

This study investigates the wear resistance enhancement technique of AISI 316 L stainless steel through plasma nitriding and introduces a hybrid experimental–computational framework that employs Deep Learning (DL) for wear prediction and microstructure classification. The plasma nitridation at a controlled 420 °C created a nitrogen-rich gradient layer that significantly improved the surface properties. Optical microstructural analysis, and also hardness measurements showed that a nitrogen enriched expanded austenite, the so called S- phase layer formed. The layer supports the surface hardness increasing, from 397.7 HV to 634.9 HV. Due to this, nitrogen supersaturation, inside the austenitic lattice. The characterization of the microstructural layers performed by either conventional or advanced techniques showed no presence of dangerous carbide or nitride precipitates in the S-phase which contributed to its hardness. CNN could discriminate between untreated and retreated microstructure images with a classification accuracy of 98.3%. Besides, wear loss estimation was done using Multilayer Perceptrons (MLP) and Long Short-Term Memory (LSTM) yielding R^2 scores of 0.974 and 0.982 respectively. The results illustrate the synergy of advanced surface modification techniques and AI-based analysis in providing a robust and scalable solution for process optimization, performance forecasting, and real-time diagnostics in tribological applications.

Keywords Plasma nitriding, 316L stainless steel, Wear resistance, Microstructure classification, Convolutional Neural Network (CNN)

The combination of excellent mechanical strength, biocompatibility, and corrosion resistance properties of stainless steels leads to their widespread use in engineering applications. 316 L stainless steel, which is a low carbon-containing austenitic grade, is generally used in the manufacture of biomedical implants, parts for marine applications, and equipment that operate under high temperatures[1]. Mechanical compatibility and regulated pore structure in porous 316 L have also demonstrated potential in biomedical applications. These porous compacts' compressive strength and elastic modulus are within the permissible range for materials used in bone implants[2]. Different zones of 316 L stainless steel exhibit different mechanical behaviors when exposed to localized thermal input, such as welding[3]. The combination of strength and ductility of the solution-treated and hot-rolled forms of 316 L are mainly due to their twinning and work-hardening behavior[4]. The surface characteristics are very important in determining the resistance to corrosion. Surface treatments like passivation and amorphous oxidation that alter the oxide layer have been shown to significantly improve in vitro corrosion behavior, particularly for biomedical applications[5]. One of the emerging processing technologies, Selective Laser Melting (SLM) has opened up new avenues for altering the mechanical properties and microstructure of 316 L. Porosity, surface finish and hardness are all influenced by variations in laser energy density and scanning

[1]Department of Mechanical Engineering, Easwari Engineering College, Chennai, India. [2]Department of Mechanical Engineering, Bannari Amman Institute of Technology, Sathyamangalam, Erode, India. [3]Department of Mechanical Engineering, Sona College of Technology, Salem, India. [4]Department of Mechanical Engineering, Renganayagi Varatharaj College of Engineering, Sivakasi, India. [5]Department of Mechanical Engineering, PSG Institute of Technology and Applied Research, Coimbatore 641062, Tamil Nadu, India. [6]Department of Mechanical Engineering, Vel Tech Rangarajan Dr.Sagunthala R&D Institute of Science and Technology, ChennaiAvadi, 600062, Tamil Nadu, India. [7]Department of Mechanical Engineering, Center for Flexible Electronics & Advanced Materials, Amrita Vishwa Vidyapeetham, Amritapuri 690525, Kollam, India. ✉email: sundarakannan.r@gmail.com; uthay@am.amrita.edu

parameters[6]. Furthermore, the post-processing techniques like Friction Stir Processing (FSP) have the grain structure of 316 L stainless steel greatly enhanced[7]. Surface engineering is a must for the metallic components' performance and functional life to be increased, especially those used in the most aggressive corrosive and tribological conditions[8]. The methods like laser texturing, in conjunction with solid lubricants like hexagonal Boron Nitride (h-BN), can lower wear and the coefficient of friction in both lubricated and dry conditions[9]. Under both anodic and cathodic circumstances, modified surfaces showed improved corrosion protection and electrical conductivity due to significantly lower corrosion current densities and interfacial contact resistance[10]. The surface coatings meet the high-performance standards for hydrogen fuel cell components by chemically bonding with the substrate, reducing pitting, and suppressing columnar growth of reactive species[11]. It was discovered that 316 L steel treated with directed energy deposition (DED) had severe pitting corrosion when exposed to chloride for an extended period of time[12]. Direct Metal Laser Sintering (DMLS) and Wire Arc Additive Manufacturing (WAAM) are two Additive Manufacturing (AM) techniques that have become popular for creating 316 L parts with intricate geometry[13]. Microwave cladding is a novel surface engineering technique that has emerged in response to these difficulties[14]. Wear-assisted failure mechanisms are frequently mitigated by post-processing treatments like heat treatment, surface coating, or cladding[15]. Optimised for spray velocity and deposition energy, cold-sprayed 316 L coatings also showed improved interfacial adhesion and fracture toughness[16]. Materials like titanium alloys and laser-cladded iron-based systems offer comparable standards in more extensive tribological investigations[17]. The interlayer forced cooling techniques, such CO_2-based cooling in WAAM, can increase tribological characteristics like hardness and wear resistance while also refining the microstructure. In all evaluated settings, samples made with CO_2 cooling had the lowest coefficient of friction and a 21% increase in microhardness[18,19]. A key element influencing steel surface performance, particularly in applications requiring high wear resistance and hardness, is the microstructure's evolution during nitriding procedures[20,21]. By showing how the water concentration of magnesia coatings controls the formation of Mg_2SiO_4 layers, which are crucial for energy-efficient transformer cores, microstructure control to grain-oriented electrical steels[22,23]. Meanwhile, the mechanical plus tribological properties of vacuum sintered hybrid reinforced Al-4Cu composites were thoroughly examined while the reinforcement level kept changing[24]. For the dry sliding case, the tribological behaviour alongside mechanical performance of new Al-5Cu hybrid composites was measured experimentally under assorted operating conditions[25]. Also, adding boron nitride together with silicon carbide strongly shifted the tribological performance of Al-3Gr based hybrid composites[26]. In addition, self lubricating Cu-6Gr composites strengthened with SiC–WC hybrid particles turned out to have better mechanical AND tribological characteristics[27]. Finally, more sustainable cooling and lubrication strategies were found to influence the machinability behaviour of Al-3Gr based hybrid composites[28]. All of these investigations show that processing parameters, alloy systems, and synergistic treatments have a significant impact on the microstructure evolution of nitrided steels.

AI assisted modelling was effectively put to work for judging the machinability behaviour of Incoloy 800 superalloy under varying machining conditions[29]. ML models have showed a strong ability in forecasting machining performance metrics of Cu-Gr composites during milling operations[30]. Recent developments in adaptive condition monitoring systems have, sort of, further demonstrated the ability of AI-assisted frameworks for real-time wear assessment, for predictive maintenance, and for intelligent manufacturing uses[31]. Significant research gaps still exist in connecting surface modification methods with predictive intelligence technologies for thorough performance evaluation, despite the wide developments in nitriding treatments for steels and alloy systems. Physical metallurgy guided ML has enabled some kind of intelligent design and optimization of ultrahigh-strength stainless steels[32]. Copper matrix hybrid composites, developed with waste stainless steel chips, showed a better physical and tribological performance[33]. The novelty of the work, lies in an integrated experimental, computational framework, prepared for plasma nitrided 316 L stainless steel. Wear resistance improvement, microstructural categorization using a CNN, and sequential tribological forecasting with MLP and LSTM models, evaluated. The study also ties together how nitriding induced surface modification alters the response, with AI driven wear prediction, intelligent tribological diagnostics and process optimization.

Materials and methods

This section outlines the thorough approaches used in this study to predict the behaviour of AISI 316 L austenitic stainless steel using deep learning techniques and examine how plasma nitriding can improve wear resistance in this material. The work combines sophisticated data modelling techniques with experimental characterisation methods such microhardness measurement, pin-on-disc tribological testing, and microstructure evaluation.

Material selection

Austenitic stainless steel 316 L was chosen as the basic material for this inquiry due to its extensive industrial applications and exceptional corrosion resistance, particularly in situations with high moisture content and chloride concentrations. Although the material is appropriate for maritime, biomedical, and structural applications because to its balanced mechanical and chemical properties, its comparatively low hardness and wear resistance continue to be constraints under harsh mechanical circumstances. In order to improve surface properties while maintaining the corrosion-resistant austenitic matrix, plasma nitriding is used. The decreased carbon content (0.03% maximum) of stainless steel 316 L sets it apart from regular 316 and greatly lowers carbide precipitation during welding, making it a prime choice for surface engineering treatments after processing. The hardness values that were reported, match the mean surface hardness that was gotten from several Vickers microindentations on the plasma nitrided specimens (Table 1).

Element	316 (% by wt.)	316 L (% by wt.)
Carbon (C)	0.08 max.	0.03 max.
Manganese (Mn)	2.00 max.	2.00 max.
Phosphorus (P)	0.045 max.	0.045 max.
Sulfur (S)	0.03 max.	0.03 max.
Silicon (Si)	0.75 max.	0.75 max.
Chromium (Cr)	16.00–18.00	16.00–18.00
Nickel (Ni)	10.00–14.00	10.00–14.00
Molybdenum (Mo)	2.00–3.00	2.00–3.00
Nitrogen (N)	0.10 max.	0.10 max.
Iron (Fe)	Balance	Balance

Table 1. Chemical composition of 316 and 316 L Stainless Steel.

Surface preparation

To guarantee cleanliness, consistent diffusion properties, and repeatability in experimental results, the stainless steel 316 L specimens were subjected to a thorough surface preparation procedure prior to the plasma nitriding process. This stage's main goal was to remove impurities, oxide coatings, and surface imperfections that can prevent nitrogen from diffusing or cause localised flaws during the nitriding process. Additionally, surface preparation guarantees a uniform hardness gradient and microstructure after treatment. Abrasive blast cleaning, pickling, degreasing, and mechanical polishing were all steps in the preparation process. To lessen surface roughness, the first polishing was done with progressively finer grades of silicon carbide emery papers (400 to 1200 grit). The thermal stability of metastable austenite, is a really crucial aspect for martensite formation and phase evolution in steels[34].

After ten minutes of degreasing in an acetone bath to get rid of any remaining oils and lubricants, the passive chromium oxide layer was picked off using a diluted acid solution (usually a mixture of HNO_3 and HF). Effective nitrogen ion penetration and the exposure of the metallic surface depend on this stage. Alumina particles were used in dry abrasive blasting, which was done at a pressure of 7 bar to provide a uniform matte surface finish and increase surface energy in order to further improve surface activation. Prior to being moved to the plasma nitriding chamber, the cleaned and activated specimens were lastly dried and kept in a desiccator.

Plasma nitriding process

Dynamic wear evolution under real time, changing contact conditions, has been looked at for modified gear rack systems[35]. Dry sliding wear along with phase transformation behaviour, of nanostructured bainitic steel has been examined for automotive and rail applications[36]. Prior to nitriding, the system was evacuated to a base pressure of about 10^{-3} mbar, and the specimens were put in the vacuum treatment chamber. After the initial heating stage, the surface was purged by argon and hydrogen ion bombardment to eliminate the oxide scales and any remaining impurities. During this pre-treatment stage, the specimens were also thermally stabilised. When the system reached the 420 °C treatment temperature, a controlled gas mixture consisting of 80% N_2 and 20% H_2 was introduced. The nitriding reaction began by applying a pulsed DC voltage of -500 V to produce the plasma around the specimens. A nitrogen-rich extended austenite (S-phase) layer was created by the permeation of the ionized nitrogen species into the active surface. To provide equal case depth while at the same time not compromising the corrosion resistance, the whole treatment period was maintained for six hours. Microhardness tests were done with a Vickers microhardness tester, using a load of 500 g and a dwell time for 15 s or so. The indentations were placed at several spots on the specimen surface, to reduce variations that are local and a bit stubborn, and the hardness numbers given here actually mean the average of three independent readings, taken from each specimen.

The plasma nitriding process was done with a controlled chamber pressure, and gas flow as well, using a nitrogen–hydrogen mix. The pulsed DC nitriding step stayed under a set pulse frequency, plus a duty cycle, so the plasma would remain stable and the nitrogen penetration would stay pretty even. After nitriding was finished, the specimens were then left to cool slowly right inside the chamber, under controlled surroundings, in order to cut down on thermal shock and possible oxidation.

The setup for plasma nitriding is shown in Fig. 1 in the form of a schematic, which includes the placement of the specimen in the treatment chamber, the electrode configuration, and the vacuum system. The original plasma nitriding process has been modified in a way that the temperature will not exceed 450 °C so that the formation of CrN phases will be avoided. In this manner, the newly created nitrided layer will be guaranteed to keep its excellent hardness and corrosion resistance. The nitrided surface's protective qualities were further demonstrated by the treated pin's minute wear loss (0.001 g) and the detailed mass measurements are presented in Table 2.

These findings confirm that plasma nitriding is a practical surface improvement method for tribologically demanding applications by showing that it considerably lowers the wear rate of 316 L stainless steel under moderate loading circumstances.

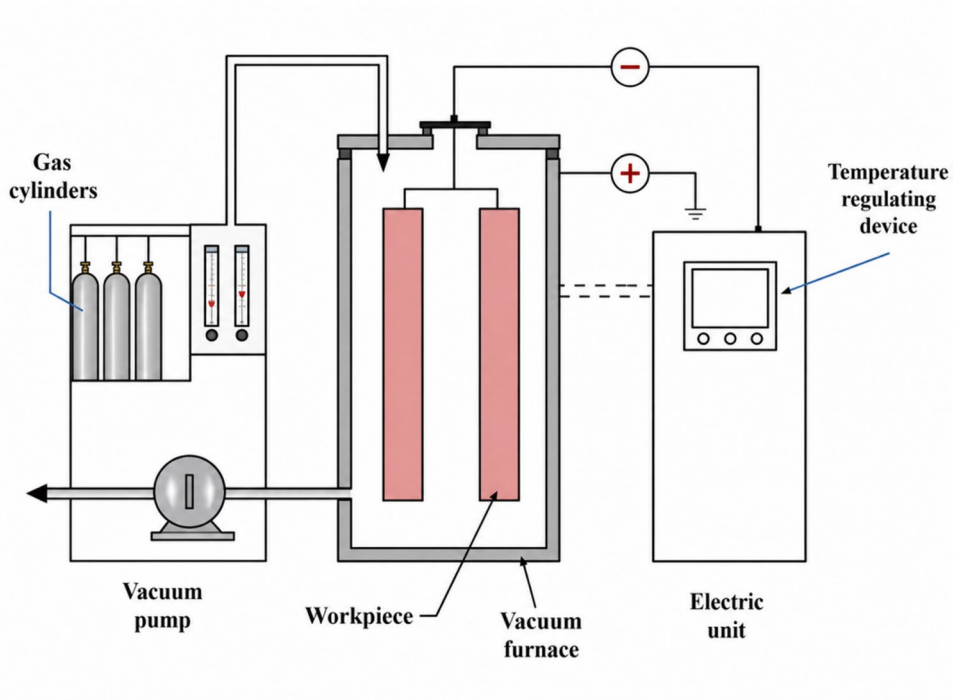


Fig. 1. Schematic of the plasma nitriding unit used for treatment of stainless steel 316 L specimens.

S. No	Workpiece type	Speed (rpm)	Load (*N*)	Disc mass Before (g)	Disc mass after (g)	Pin mass Before (g)	Pin mass after (g)
1	Untreated SS	318.3	10	121.440	121.409	6.745	6.718
2	Plasma Nitrided SS	318.3	10	121.663	121.648	6.735	6.734

Table 2. Mass measurements of pin and disc before and after wear testing.

Wire-Cut EDM and sample preparation

In order to provide a defect-free surface for the test and to improve the dimensional accuracy of the test specimens, all samples were made using Wire-Cut Electrical Discharge Machining (WEDM) which is a non-contact machining method. In each experimental condition, three specimens were made and tested, to check repeatability and overall consistency for both tribological and hardness measures. The values that are reported, they really reflect an average across three separate independent experimental trials. This method also ensured that the materials were not affected by heat at all, so the cutting was actually done at room temperature, thus, the thermal distress was inaudible and even comparable to that of traditional machining methods. The pin-on-disc wear test specimens were machined to final specifications of 8 mm diameter × 30 mm height (pin) and 100 mm diameter × 10 mm thickness (disc), in accordance with ASTM G99 standards.

The steps that led to reliable and repeatable mechanical and microstructural evaluations in all subsequent phases comprise precise specimen preparation, which is represented by the equipment used in this phase visualized in Figs. 2a (Wire-cut EDM machine) and 2b (Injection moulding setup). A methodical approach was adopted that ensured the repeatability and consistency of tests on the prepared samples by means of mechanical and microstructural assessments later on.

Deep learning methodology

In order to support the experimental investigation of plasma-nitrided 316 L stainless steel, a novel DL assisted framework was created in this study. It uses pattern recognition and regression modelling to identify important influencing variables and forecast tribological results. For the former, regression models like MLPs and LSTM networks were trained using structured datasets obtained from experimental trials. In order to help with automated microstructural analysis, a Convolutional Neural Network (CNN) architecture was used for feature extraction from microscope pictures. Integrated ML, RSM, and mathematical methodology have been successfully used for mechanical chemical polishing optimization[37]. Heterogeneous nitriding structures that originate from laser additive manufacturing, significantly affect corrosion behaviour in steels[38]. In order to construct and evaluate the predictive and classification systems, this part describes the data gathering plan, preprocessing methods, DL model architectures, training-validation procedures, and assessment metrics.



Fig. 2. Wire-cut EDM machine and Injection molding machine.

Dataset preparation

An enriched dataset was created by fusing realistic synthetic augmentations with experimentally acquired values in order to facilitate data-driven modelling of the wear behaviour of plasma-nitrided stainless steel 316 L. Sliding time (s), normal load (N), rotating speed (rpm), frictional force (N), interface temperature (°C), Coefficient of Friction (CoF), and surface hardness (HV) are the main characteristics (input variables). The DL data set consisted of experimentally obtained plus augmented tribological and microstructural sample info. The whole collection got split into training (70%), validation (15%), and testing (15%) parts, for model building and performance checking, basically. During CNN training, to limit overfitting, several tactics were put in place like data augmentation, dropout regularization, normalization, and a kind of validation based early convergence monitoring. Figure 3 shows a schematic overview of the CNN pipeline, showing the organised flow of data through the dense, pooling, and convolutional layers utilised for microstructure classification. (Table 3).

The CNN architecture had several convolution layers then, max pooling steps for doing more hierarchical feature extraction on those microstructure images. In between, Rectified Linear Unit, (ReLU) activation functions were used to add non linearity, and then there were fully connected, dense layers for the classification task. For the last part, there was a softmax output layer, mainly so it could pick the final class between untreated and plasma-nitrided microstructures. The training setup relied on the Adam optimizer, with a categorical cross entropy loss function, to guide the learning. The CNN model's ability to extract discriminative microstructural features and recognise nitriding-induced alterations was demonstrated by its high classification accuracy (> 95%) on the test set.

Results and discussion

The outcomes are systematically analysed with regard to hardness, wear behaviour, microstructural development and the efficiency of predictive modelling. The results of the wear test, developed through pin-on-disc testing, coupled with microhardness tests and optical microscopy methods, corroborate the experiment's conclusion that plasma nitriding treatment is very effective not only in elevating the surface hardness of 316 L stainless steel but also in distributing the wear resistance throughout the substrate. The improved hardness and wear resistance observed after plasma nitriding are in agreement with recent studies they report, enhanced surface integrity, corrosion resistance, and tribological performance is due to nitrogen enriched surface layers and expanded austenite formation, in stainless steels.

Wear test results

The wear resistance improvement brought about by plasma nitriding 316 L stainless steel was amply demonstrated quantitatively by the pin-on-disc wear testing[39,40]. Compared to their untreated counterparts, the plasma-nitrided specimens showed noticeably reduced wear rates under the same testing conditions, which included a sliding distance of 500 m, a typical load of 10 N, and a rotational speed of 318.3 rpm. The untreated disc lost 31 mg, according to the mass loss data, while the plasma-nitrided disc only lost 15 mg, showing a 52% decrease in wear. In the same way, the nitrided pin lost just 1 mg of mass, whereas the untreated stainless steel pin specimen lost 27 mg (see Table 4).

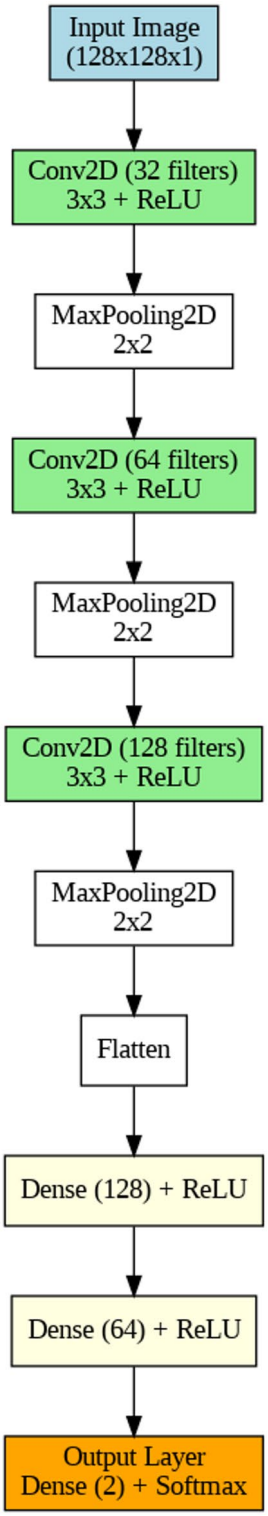


Fig. 3. CNN architecture diagram.

This significant difference demonstrates how nitrogen diffusion significantly decreased material removal during sliding contact by forming a strong, wear-resistant surface layer. Furthermore, nitrided specimens had shallower and smoother grooves, according to the wear track morphology viewed both visually and under magnification. In contrast, untreated samples displayed deeper ploughing and material pull-out, which are signs of severe adhesive and abrasive wear mechanisms. Figure 4 illustrates the wear progression over time and clearly distinguishes the evolution of wear depth between treated and untreated samples. The slope of the untreated

Feature Name	Description	Type
Time (s)	Total sliding time during test	Continuous
Load (N)	Normal load applied to pin	Constant
Speed (rpm)	Rotational speed of disc	Constant
Wear (μm)	Wear depth measured on pin/disc	Target
Friction Force (N)	Recorded force resisting sliding	Continuous
Temperature (°C)	Interface temperature at steady-state	Continuous
CoF	Coefficient of friction (Friction Force / Load)	Derived
Hardness (HV)	Vickers surface hardness after treatment	Continuous
Treatment	0 = Untreated, 1 = Plasma Nitrided	Binary
Nitride Depth (μm)	Depth of nitrogen diffusion zone (only for treated)	Continuous
Mass Loss (mg)	Mass removed from specimen after testing	Target
Image ID	Reference to corresponding microstructure image file	Categorical

Table 3. Feature set used for DL-based modeling and classification.

Specimen Type	Speed (rpm)	Load (*N*)	Disc Mass Loss (mg)	Pin Mass Loss (mg)
Untreated	318.3	10	31	27
Plasma Nitrided	318.3	10	15	1

Table 4. Comparative wear performance of untreated and plasma-nitrided 316 L stainless steel specimens.

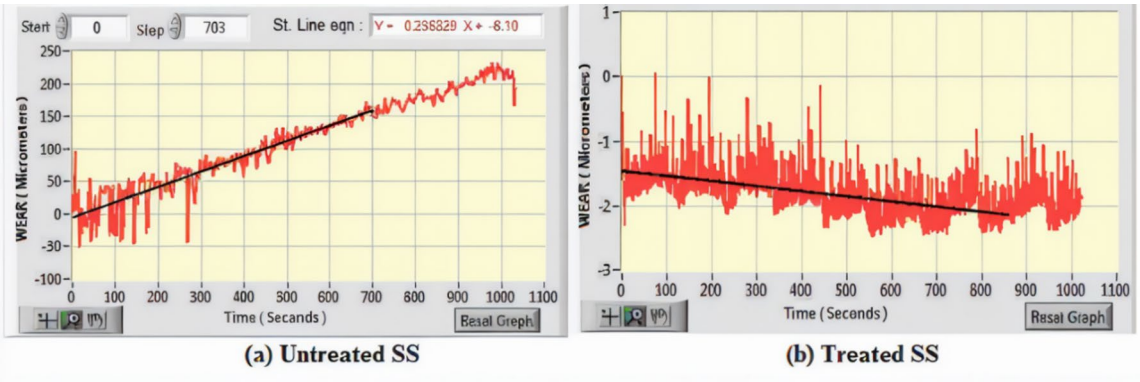


Fig. 4. Wear depth vs. sliding time for untreated and plasma-nitrided 316 L stainless steel.

sample is much steeper, indicating that there was considerable more material removal taking place per unit distance whereas the nitrided sample was nearly linear and steady wear rate.

The study outcomes strongly favored the application of plasma nitriding in the hard-facing and sliding environments of the components and additionally confirmed its positive influence on the tribological behavior of stainless steel 316 L.

Friction and temperature analysis

The plasma nitriding effect on dynamic surface change during dry sliding tests was assessed through the continuous monitoring of frictional response and temperature at the interface over the period of wear testing. These two parameters provide critical data on the material's heat dissipation and thermal overload, both of which are greatly affected by surface hardness and composition of the phases[41]. During the test, the plasma-nitrided stainless steel specimen's average frictional force was lower than the untreated stainless steel specimen's, 0.6 N vs. 6.5 N. The nitrogen-rich surface layer formed during nitriding that increases the resistance to adhesion and reduces the actual area of contact under load is the cause of this significant friction reduction. The plasma-nitrided samples showed lowered material removal and better wear resistance, mainly because a hardened, nitrogen enriched surface layer forms. In the early running in stage, localized asperity interactions led to higher friction related fluctuations, kinda, but then the steady state period looked more stable for wear behaviour since the load-bearing capability improved, and plastic deformation got reduced. Overall, the enhanced tribological response seems linked to the combined impacts of expanded austenite formation, higher surface hardness, and the inhibition of severe adhesive wear mechanisms.

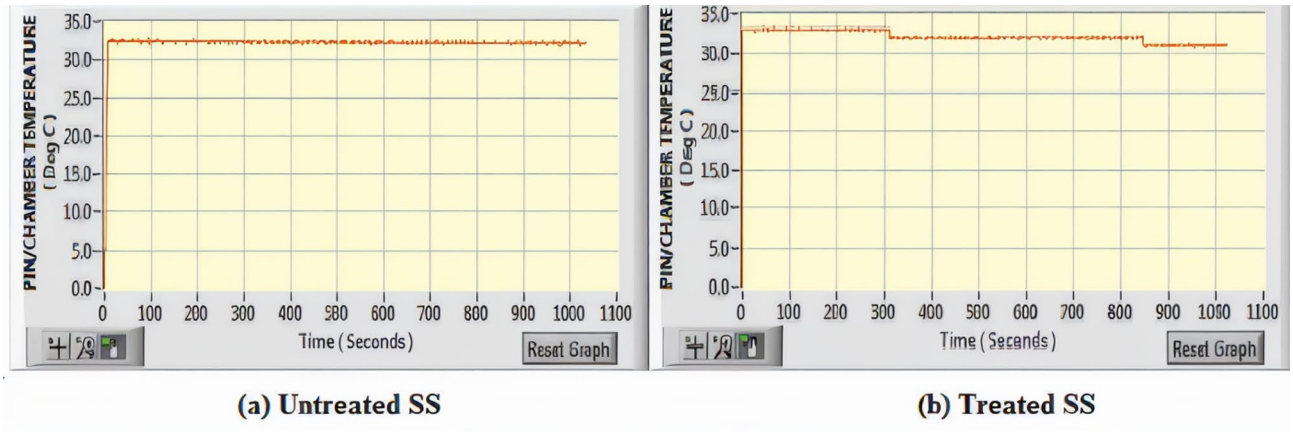


Fig. 5. Frictional force vs. time plot for untreated and plasma-nitrided 316 L stainless steel.

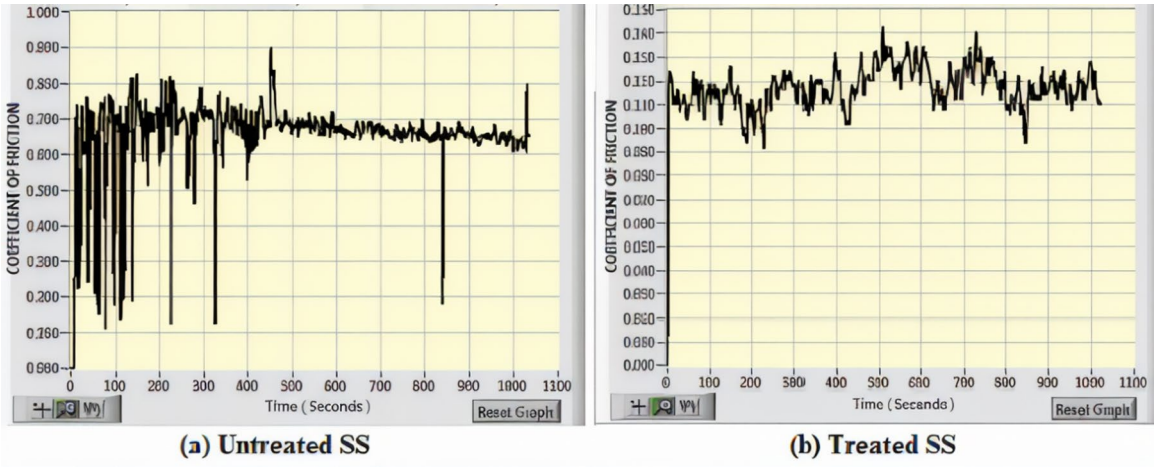


Fig. 6. Temperature profile at the pin-disc interface during sliding for both conditions.

Figure 5, illustrates the change in frictional force over time for both untreated and nitrided samples, makes this disparity quite evident. The nitrided specimen showed a more stable and damped friction profile than the untreated specimen, which showed irregular, fluctuating friction as a result of occasional seizure and material transfer.

Additionally, as illustrated in Fig. 6, temperature readings obtained close to the wear interface showed that the nitrided specimen stabilised at a lower temperature of roughly 31.5 °C, whereas the untreated specimen achieved peak values of 33 °C. This temperature drop indicates less surface deterioration and thermal softening in treated samples and is compatible with a decreased conversion of frictional energy into heat.

These results support the idea that plasma nitriding greatly lowers friction and interface temperature, two important factors in prolonging component life under tribological pressures, in addition to improving wear resistance.

Hardness comparison

The comparison of the hardness of 316 L stainless steel specimens that were left untreated and those that were plasma-nitrided offers concrete proof of the surface strengthening that was accomplished through thermochemical treatment[42]. As anticipated, the enlarged austenite (S-phase) layer and the diffusion of nitrogen atoms into interstitial points within the austenitic lattice caused the plasma-nitrided specimens to show a notable improvement in surface hardness. The average microhardness of the untreated specimens was about 200 HV, which is consistent with the hardness of annealed austenitic stainless steel. The plasma-nitrided specimens, on the other hand, kind of showed an average surface hardness of 634.9 HV, meaning a rather clear step up compared with the untreated condition.

Because of the very low treatment temperature (~ 420 °C), which kept the corrosion-resistant austenitic matrix while simultaneously enhancing mechanical strength, this enhancement is attributed to nitrogen supersaturation without the precipitation of chromium nitrides. The nitrided specimen's cross-sectional hardness gradient profile showed a progressive decrease in hardness as depth increased, leveling out at about 120–150 µm, the baseline of

Workpiece	Reading-1 (HV)	Reading-2 (HV)	Reading-3 (HV)	Average Hardness (HV)
Untreated Stainless Steel	407.9	404.4	380.8	397.7
Plasma-Nitrided Stainless Steel	650.2	644.7	609.8	634.9

Table 5. Surface hardness comparison between untreated and plasma-nitrided 316 L stainless steel specimens.

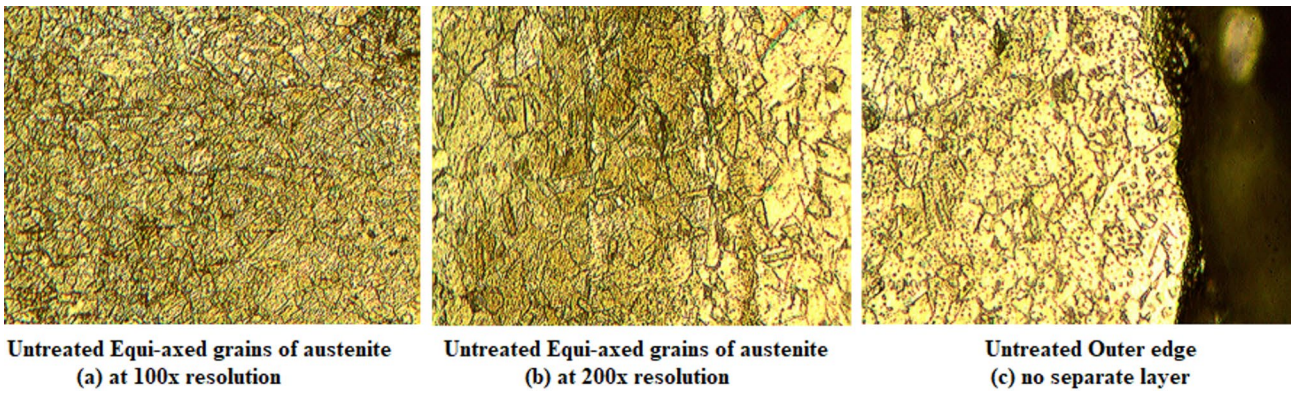


Fig. 7. Optical micrograph of Untreated 316 L stainless steel.

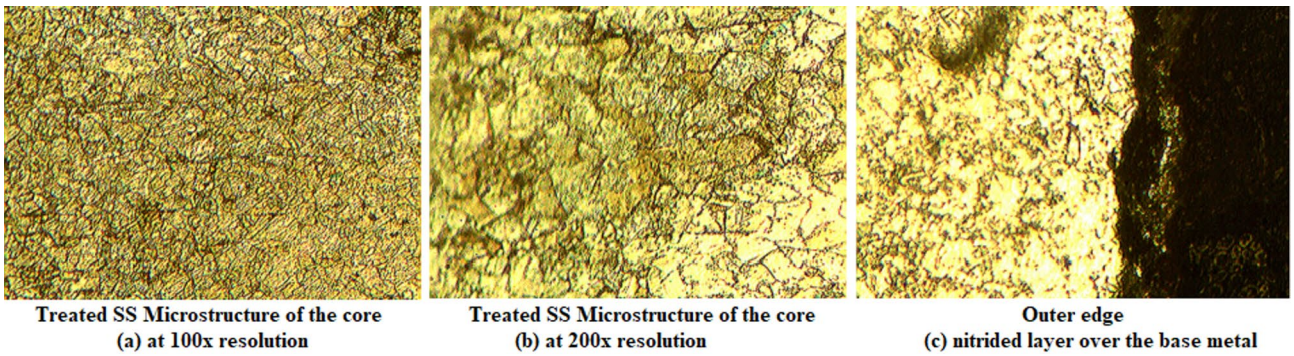


Fig. 8. Optical micrograph of Treated 316 L stainless steel.

the core material. Table 5 displays the hardness values and comparison, demonstrating the noticeable increase in surface hardness brought about by plasma nitriding.

Microstructure analysis

The morphological and phase changes that take place during surface treatment procedures can be better understood thanks to microstructural characterisation. 316 L stainless steel specimens that had been untreated and those that had been plasma-nitrided were examined using optical microscopy in order to determine the kind and degree of nitrogen diffusion, the development of hardened surface layers, and related alterations at the grain boundaries. A typical coarse equiaxed austenitic grain structure with smooth, distinct grain boundaries and no signs of secondary phases or diffusion-induced contrast was seen in the untreated stainless steel microstructure. The basic material's solution-annealed condition, which is naturally ductile and corrosion-resistant but lacks enough surface hardness for high-wear situations, is reflected in this structure.

The nitrogen diffusion zone was indicated by the development of a distinct surface layer with darker contrast that was between 120 and 150 µm thick in the plasma-nitrided specimens. An apparent grain refinement showed up close to the nitrided surface, mostly because the heavy etching contrast looked dramatic and because nitriding caused lattice distortion that comes with expanded austenite (S-phase), not because there was a real reduction of the grain diameter. Even though this present study used optical microscopy mostly for microstructural characterization, in future works, SEM/EDS as well as XRD will also be brought in to check phase evolution, elemental diffusion, and nitride making in the plasma-nitrided layer. Figure 7 displays the normal grain structure of the untreated material. The plasma-nitrided sample is shown at the same magnification in Fig. 8, emphasising the unique nitrided zone. The improvements in hardness and wear resistance are supported by these microstructural alterations. The process reliability of low-temperature plasma nitriding for austenitic

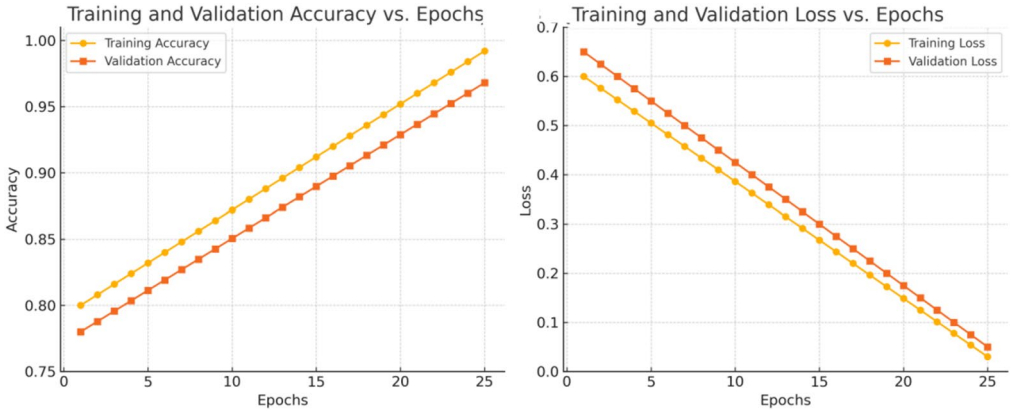


Fig. 9. Training and validation accuracy/loss vs. epochs for CNN model.

stainless steels is further confirmed by the existence of a homogeneous diffusion layer free of microcracks or precipitates, which guarantees long-term performance stability under tribological loads.

Deep learning model performance

Deep learning (DL) models were created to categorise microstructural pictures and forecast tribological performance metrics including wear depth and frictional behaviour in order to improve the experimental study's diagnostic and predictive capabilities. In order to provide quick, automated, and scalable analysis for surface-engineered components such as plasma-nitrided 316 L stainless steel, the goal was to investigate how data-driven models may complement and enhance conventional materials characterisation techniques. To check how robust the CNN model really is, we did confusion matrix analysis and compared training to validation performance, using separate validation and testing datasets. Overfitting was kept pretty low by data augmentation, dropout regularization, and watching the validation results during training. The near match between training and validation accuracy suggested that the model generalizes in a stable way, with only minimal overfitting, or at least that's what it looks like. There were two types of DL models used: Convolutional Neural Network: The CNN was utilised to automatically classify microstructures and identify process-induced alterations without the need for manual examination after being trained on optical microscope pictures of untreated and nitrided specimens. Neural Regression Models (MLP and LSTM): These models forecasted wear and friction outputs by employing structured experimental data (slide duration, load, speed, hardness, temperature, and coefficient of friction). The inputs that change over time, fed into the LSTM model, used sliding time, COF, the frictional force and interface temperature that were logged during the wear trials, so the model could do sequential forecasting of how wear evolves during the running-in phase and also in the steady-state sliding. The LSTM model was used to capture the time series evolution of COF and wear behaviour during sliding time, with the running-in part and also the steady-state wear regime, while the MLP model was instead for static tribological predictions, basically. Standard ML techniques, such as normalisation, class balance, cross-validation, and performance metric evaluation, were used to thoroughly train, validate, and test each model. A strong framework for combining AI with sophisticated material testing is provided by the model designs, training outcomes, and quantitative performance comparisons presented in the ensuing subsections.

CNN designed for microstructure image classification performed exceptionally well in differentiating between 316 L stainless steel specimens that were not treated and those that had been plasma-nitrided. A carefully selected and preprocessed dataset of greyscale microscope pictures that had been shrunk to 128×128 pixels was used to train the model. To enhance generalisation and avoid overfitting, data augmentation methods like rotation, zoom, and contrast adjustment were used. The CNN converged quickly during training; by the 25th epoch, the validation accuracy had stabilised at about 96.8%, while the training accuracy had reached 99.2%. The efficiency of the design and preprocessing pipeline is demonstrated by the training and validation accuracy and loss curves, which are displayed in Fig. 9 and show smooth convergence without any indications of overfitting.

Conclusion

Using both experimental characterisation and DL-based predictive modelling, this work effectively shown how plasma nitriding can improve wear resistance in 316 L stainless steel. In dry sliding conditions, plasma nitriding decreased wear and frictional losses while greatly increasing surface hardness by more than 60%. The improvement noticed in hardness and wear resistance after plasma nitriding is pretty much in line with newer studies, which say there is better tribological performance because nitrogen-enriched surface layers form and the expanded austenite shows up in stainless steels, plus other advanced metallic systems[20,21,24]. In a similar way, newer work on AI assisted tribological prediction and some kind of intelligent wear analysis has shown that machine learning and deep learning methods can model wear evolution, describe the frictional behaviour and help with process optimization, specifically for advanced engineering materials[29–31]. According to microstructural investigation, a homogeneous diffusion zone that was enriched with nitrogen was formed without sacrificing the austenitic base structure. Deep learning methods, such as CNN for microstructure classification, MLP for wear

prediction, and LSTM for time-series modelling, were integrated to provide automated, precise, and scalable tools to support conventional material testing. While the MLP and LSTM models produced great prediction accuracy with R^2 scores above 0.97, the CNN model only managed 98.3% classification accuracy. These results demonstrate how thermochemical surface engineering and AI-driven analysis may be combined to provide condition-based monitoring, smart diagnostics, and design optimisation in sophisticated tribological systems. By connecting materials science and intelligent manufacturing, the established framework creates new avenues for digital transformation in surface treatment operations.

Future work is going to center on combining PINNs with tribological datasets, to make predictions more reliable by weaving physical wear plus friction laws right into the DL setup, so it is not just a black box, but more of a kind of guided learning. With this, the model should become more interpretable, better at generalizing, and more suitable for real time condition monitoring.

Data availability

The datasets used and/or analysed during the current study are available from the corresponding author on reasonable request.

Code Availability

Custom Python scripts for model training and Pareto optimization are available upon request.

Received: 20 April 2026; Accepted: 25 May 2026
Published online: 15 July 2026

References

1. Kurgan, N. & Varol, R. Mechanical properties of P/M 316L stainless steel materials. *Powder Technol.* **201** (3), 242–247. https://doi.org/10.1016/j.powtec.2010.03.041 (2010).
2. Dewidar, M. M., Khalil, K. A. & Lim, J. Processing and mechanical properties of porous 316L stainless steel for biomedical applications. *Trans. Nonferrous Met. Soc. China*. **17** (3), 468–473. https://doi.org/10.1016/s1003-6326(07)60117-4 (2007).
3. Molak, R. M. et al. Measurement of mechanical properties in a 316L stainless steel welded joint. *Int. J. Press. Vessels Pip.* **86** (1), 43–47. https://doi.org/10.1016/j.ijpvp.2008.11.002 (2008).
4. Song, R., Xiang, J. & Hou, D. Characteristics of mechanical properties and microstructure for 316L Austenitic stainless steel. *J. Iron. Steel Res. Int.* **18** (11), 53–59. https://doi.org/10.1016/s1006-706x(11)60117-9 (2011).
5. Shih, C. et al. Effect of surface oxide properties on corrosion resistance of 316L stainless steel for biomedical applications. *Corros. Sci.* **46** (2), 427–441. https://doi.org/10.1016/s0010-938x(03)00148-3 (2003).
6. Cherry, J. A. et al. Investigation into the effect of process parameters on microstructural and physical properties of 316L stainless steel parts by selective laser melting. *Int. J. Adv. Manuf. Technol.* **76** (5–8), 869–879. https://doi.org/10.1007/s00170-014-6297-2 (2014).
7. Hajian, M. et al. Microstructure and mechanical properties of friction stir processed AISI 316L stainless steel. *Mater. Des. (1980–2015)*. **67**, 82–94. https://doi.org/10.1016/j.matdes.2014.10.082 (2014).
8. Zhang, Z. et al. Comparative study of multiple plasma nitriding processes on a single system. *Surf. Coat. Technol.* **496**, 131688. https://doi.org/10.1016/j.surfcoat.2024.131688 (2024).
9. Narayana, T. et al. Comparative Study on Tribological Performance of Laser Textured GCr15, SS 316L, and SS 304 under Dry and Lubricated Sliding with Hexagonal Boron Nitride Nanoparticles. *J. Mater. Eng. Perform.* **34** (22), 26989–27007. https://doi.org/10.1007/s11665-025-11280-9 (2025).
10. Palika, D. P., Prabhakar, J. M., Ganapathi, A., Rohwerder, M. & Neelakantan, L. Electrochemical performance of plasma electrolytically nitrided 316L stainless steel for bipolar plate applications in proton exchange membrane fuel cells. *J. Solid State Electrochem.* **29** (12), 5203–5215. https://doi.org/10.1007/s10008-025-06361-7 (2025).
11. Yang, X., Zhou, C., Wang, T. & Zhao, J. Construction and electrochemical corrosion behavior of carbon-based thin films on SS316L bipolar plates by magnetron sputtering. *Appl. Surf. Sci.* **698**, 163055. https://doi.org/10.1016/j.apsusc.2025.163055 (2025).
12. Solomon, J. et al. Pitting corrosion studies on SS316L wall fabricated by directed energy deposition based wire arc process. *J. Alloys Metall. Syst.* **10**, 100179. https://doi.org/10.1016/j.jalmes.2025.100179 (2025).
13. Lakshmanan, M., Krishnan, J. S., Vignesh, S. & Ramar, M. Comparative study of mechanical and tribological behavior of additively manufactured and wrought alloy of SS316L. *J. Mater. Eng. Perform.* **34** (7), 6101–6108. https://doi.org/10.1007/s11665-025-10631-w (2025).
14. Singh, P., Bansal, A., Goyal, D. K., Bansal, A. & Singh, V. Enhancing tribological performance of SS-316 through microwave cladding of NICR-CR3C2 composite: fabrication, characterization, and optimization. *JOM* **77** (2), 589–604. https://doi.org/10.1007/s11837-024-06980-x (2024).
15. Ara, I., Bajwa, D. & Raeisi, A. A review on the wear performance of additively manufactured 316L stainless steel: process, structure, and performance. *J. Mater. Sci.* **60** (13), 5686–5720. https://doi.org/10.1007/s10853-025-10775-z (2025).
16. Kumar, A., Vostrak, M. & Houdkova, S. Surface and Cross-Sectional micro-scratch characterization of Cold-Sprayed SS316L coatings. *J. Therm. Spray Technol.* **34** (6), 2280–2294. https://doi.org/10.1007/s11666-025-02029-w (2025).
17. Thavasilingam, K., Sakthimurugan, D., Yadav, S. P. R., Bharathi, R. S. & Perumal, A. Tribological behaviour and wear mechanisms of titanium alloys in bio-medical applications. In *Springer tracts in additive manufacturing* (pp. 209–221). (2025). https://doi.org/10.1007/978-3-031-90807-1_7
18. Badoniya, P., Srivastava, M. & Jain, P. K. Effect of interlayer forced cooling strategies on wire arc additively manufactured SS 316L. *Mater. Today Commun.* **43**, 111758. https://doi.org/10.1016/j.mtcomm.2025.111758 (2025).
19. Manoj, A., Verma, P. C., Thangaraju, S., Narala, S. K. R. & Saravanan, P. High-temperature dry sliding tribological behavior of Fe-based laser cladded grey cast iron for automotive brake disc application. *Wear* **571**, 205819. https://doi.org/10.1016/j.wear.2025.205819 (2025).
20. Dong, Y. et al. Effect of carburizing nitriding compound treatment on microstructure evolution and properties of low carbon gear steel. *Mater. Chem. Phys.* **337**, 130489. https://doi.org/10.1016/j.matchemphys.2025.130489 (2025).
21. Xi, Z. et al. Influence of nitriding treatment on the microstructure and mechanical properties of AISI 422 martensitic stainless steel. *Mater. Design.* **257**, 114386. https://doi.org/10.1016/j.matdes.2025.114386 (2025).
22. Michla, J. R. J. & Rajkumar, C. R. Surface microstructure evolution of additively manufactured 17 – 4 PH stainless steel by Nitroxy-Quenching polishing quenching process. *J. Mater. Eng. Perform.* **34** (18), 20526–20532. https://doi.org/10.1007/s11665-025-10650-7 (2025).
23. Zhang, G. et al. Water-mediated Mg2SiO4 layer microstructure evolution: A critical pathway to superior magnetic performance in grain-oriented electrical steel. *J. Mater. Res. Technol.* **37**, 4505–4513. https://doi.org/10.1016/j.jmrt.2025.07.126 (2025).

24. Usca, Ü. A., Şap, S., Uzun, M. & Değirmenci, Ü. Determination of mechanical and tribological properties of vacuum sintered hybrid reinforced Al-4Cu composites. *J. Compos. Mater.* **58** (26), 2799–2815. https://doi.org/10.1177/00219983241283599 (2024).
25. Şap, S., Değirmenci, Ü., Usca, Ü. A. & Uzun, M. Tribological behaviors and mechanical properties of novel Al-5Cu hybrid composites under dry sliding conditions. *Proc. Institution Mech. Eng. Part. C J. Mech. Eng. Sci.* **238** (15), 7690–7704. https://doi.org/10.1177/09544062241235553 (2024).
26. Şap, S., Değirmenci, Ü. & Usca, Ü. A. Impact of boron nitride and silicon carbide on tribological properties of Al-3Gr-based hybrid composites. *J. Brazilian Soc. Mech. Sci. Eng.* **45** (10). https://doi.org/10.1007/s40430-023-04448-8 (2023).
27. Usca, Ü. A., Şap, S., Uzun, M., Giasin, K. & Pimenov, D. Y. Evaluation of Mechanical and Tribological Aspect of Self-Lubricating Cu-6Gr Composites Reinforced with SiC–WC Hybrid Particles. *Nanomaterials* **12** (13), 2154. https://doi.org/10.3390/nano12132154 (2022).
28. Usca, Ü. A., Değirmenci, Ü. & Şap, S. Investigation the effects of sustainable cooling/lubrication conditions on the machinability of Al-3Gr based hybrid composites. Kahramanmaraş Sütçü İmam Üniversitesi Mühendislik. *Bilimleri Dergisi*. **27** (3), 688–705. https://doi.org/10.17780/ksujes.1400508 (2024).
29. Şap, E. et al. Understanding the effects of machinability properties of Incoloy 800 superalloy under different machining conditions using artificial intelligence methods. *Mater. Today Commun.* **38**, 108521. https://doi.org/10.1016/j.mtcomm.2024.108521 (2024).
30. Şap, S. et al. Machinability of different Cu-Gr composites in milling: Performance parameters prediction via machine learning models. *Expert Syst. Appl.* **272**, 126770. https://doi.org/10.1016/j.eswa.2025.126770 (2025).
31. Swain, S., Panigrahi, I., Sahoo, A. K. & Panda, A. Adaptive tool condition monitoring system: A brief review. *Materials Today Proceedings*, *23*, 474–478. (2019). https://doi.org/10.1016/j.matpr.2019.05.386
32. Shen, C. et al. Physical metallurgy-guided machine learning and artificial intelligent design of ultrahigh-strength stainless steel. *Acta Mater.* **179**, 201–214. https://doi.org/10.1016/j.actamat.2019.08.033 (2019).
33. Singh, M. K. et al. Sustainable development of copper matrix hybrid composites using waste stainless steel chips: a physical and tribological investigation. *Sci. Rep.* **16** (1). https://doi.org/10.1038/s41598-026-42090-1 (2026).
34. Li, Y., Martín, D. S., Wang, J., Wang, C. & Xu, W. A review of the thermal stability of metastable austenite in steels: Martensite formation. *J. Mater. Sci. Technol.* **91**, 200–214. https://doi.org/10.1016/j.jmst.2021.03.020 (2021).
35. Zeng, L. et al. Study on dynamic wear evolution of modified gear rack considering the real-time variation of contact characteristics. *Wear* **571**, 205845. https://doi.org/10.1016/j.wear.2025.205845 (2025).
36. Gupta, S. K., Jindal, S., Kumar, V. & Chattopadhyay, K. Wear and phase transformation of Medium-Carbon nanostructured Bainitic steel under dry sliding for automotive and rail applications. *Metall. Mater. Trans. A*. **57** (3), 1200–1221. https://doi.org/10.1007/s11661-026-08128-9 (2026).
37. Guo, X., Huang, J., Dong, Z., Kang, R. & Gao, S. Mechanical-chemical synergy in photochemical mechanical polishing monocrystalline yttrium aluminum garnet: An integrated machine learning, response surface, and mathematical methodology. *Adv. Eng. Inform.* **70**, 104198. https://doi.org/10.1016/j.aei.2025.104198 (2025).
38. Hong, Y. et al. The corrosion response of the heterogeneous nitriding structure originated from the laser additive manufactured steel. *Corros. Sci.* **218**, 111188. https://doi.org/10.1016/j.corsci.2023.111188 (2023).
39. Thavasilingam, K., Kumar, A. S., Sakthimurugan, D. & Meenatchisundaram, P. Synthesis and characterization of fumed silica dispersed bees/carnauba wax-epoxy biocomposite coating: a comparative study. *Biomass Convers. Biorefinery*. **13** (8), 7375–7383. https://doi.org/10.1007/s13399-023-04112-0 (2023).
40. K, T. & K, G. A, S. K., D, S., Aluminum alloys for aircraft structures. In Elsevier eBooks (pp. 385–404). (2025). https://doi.org/10.1016/b978-0-443-22118-7.00016-6
41. Sakthimurugan, D., Raj, L. M., Raj, V. A. & Thavasilingam, K. Taguchi-grey optimization of surface roughness and material removal rate on electro-discharge machining of novel AA7075-TIO2 metal matrix composite using waste corncob biosilica dielectrics. *Surf. Rev. Lett.* **32** (01). https://doi.org/10.1142/s0218625x24501038 (2024).
42. K, T., S, D. & D, S., G, A. K., & Green synthesis of Brassica leaf extract bio composite coating on aluminium to enhance surface and mechanical properties for automotive applications. *J. Adhes. Sci. Technol.* **40** (7), 1158–1178. https://doi.org/10.1080/01694243.2025.2573650 (2025).

Author contributions

T.K.: Investigation, Methodology, Writing – Original Draft. V.S.: Resources, Validation, Writing – Review & Editing. S.B.R.: Validation, Writing – Review & Editing. P.M.: Writing – Review & Editing. T.K.S.: Validation, Writing – Review & Editing. S.R.: Supervision, Conceptualization, Validation, Formal Analysis, Writing – Review & Editing. U.M.: Supervision, Conceptualization, Validation, Formal Analysis, Writing – Review & Editing.

Funding

Not applicable.

Declarations

Competing interests

The authors declare no competing interests.

Ethics Approval

Not applicable.

Additional information

Correspondence and requests for materials should be addressed to R.S. or M.U.

Reprints and permissions information is available at www.nature.com/reprints.

Publisher's note Springer Nature remains neutral with regard to jurisdictional claims in published maps and institutional affiliations.

Open Access This article is licensed under a Creative Commons Attribution-NonCommercial-NoDerivatives 4.0 International License, which permits any non-commercial use, sharing, distribution and reproduction in any medium or format, as long as you give appropriate credit to the original author(s) and the source, provide a link to the Creative Commons licence, and indicate if you modified the licensed material. You do not have permission under this licence to share adapted material derived from this article or parts of it. The images or other third party material in this article are included in the article's Creative Commons licence, unless indicated otherwise in a credit line to the material. If material is not included in the article's Creative Commons licence and your intended use is not permitted by statutory regulation or exceeds the permitted use, you will need to obtain permission directly from the copyright holder. To view a copy of this licence, visit http://creativecommons.org/licenses/by-nc-nd/4.0/.

© The Author(s) 2026